Nanoscale

PAPER

View Article Online
View Journal | View Issue

Cite this: *Nanoscale*, 2014, **6**, 13754

Plasmonic-enhanced Raman scattering of graphene on growth substrates and its application in SERS†

Yuan Zhao,[a] Guanxiong Chen,[a] Yuanxin Du,[a] Jin Xu,[a] Shuilin Wu,[a] Yan Qu[b,c] and Yanwu Zhu*[a,d]

Received 25th July 2014,
Accepted 12th September 2014

DOI: 10.1039/c4nr04225e

www.rsc.org/nanoscale

We detail a facile method for enhancing the Raman signals of as-grown graphene on Cu foils by depositing gold nanoislands (Au Nis) onto the surface of graphene. It is found that an enhancement of up to 49 fold in the graphene Raman signal has been achieved by depositing a 4 nm thick Au film. The enhancement is considered to be related to the coupling between graphene and the plasmon modes of Au Nis, as confirmed by the finite element simulations. The plasmonic effect of the Au/graphene/Cu hybrid platform leads to a strong absorption at the resonant wavelength whose position shifts from visible light (640 nm) to near-infrared (1085 nm) when the thickness of Au films is increased from 2 nm to 18 nm. Finally, we demonstrate that hybrid substrates are reliable surface-enhanced Raman scattering (SERS) systems, showing an enhancement factor of ~10^6 for dye molecules Rhodamine B and Rhodamine 6G with uniform and stable response and a detection limit of as low as 0.1 nM for Sudan III and Sudan IV.

1. Introduction

Graphene, a single layer of sp^2-bonded carbon atoms in a hexagonal configuration with unique optical and electronic properties, has been attracting intensive research in photonics and optoelectronics.[1–6] Techniques have been developed to meet the requirements of scientific research and product applications for synthesizing large-area, high-quality graphene films utilizing *e.g.* high-temperature sublimation of SiC,[7] reduction from graphene oxides[8] or metal-catalyzed chemical vapor deposition (CVD).[9] Specifically, large-area polycrystalline graphene films with an average grain size in the micrometer scale and a single layer coverage of more than 95% can be readily achieved on Cu foils by CVD.[10] Recently, the CVD method has been further optimized to produce graphene with grain size in the millimeter scale.[11] CVD growth of graphene on Cu substrates has been considered to be a promising approach for achieving industry-scale production of graphene due to the low cost of Cu foils and potential production in a continuous manner such as with the roll-to-roll technique.[12,13]

On the other hand, Raman spectroscopy is an efficient method to probe the structural and physical properties of graphene, such as the atomic structure of edges and the presence of disorder, defects, charge and strain.[14,15] Unfortunately the Raman signal of as-grown graphene on Cu foils is usually weak with a strong background, probably due to the surface plasmon emission of Cu arising from the transitions between electrons and holes with photoluminescence and/or the strain in graphene on Cu foils.[16,17] Otherwise graphene can be transferred onto a substrate like SiO_2/Si with processes involving chemical treatments, for it is capable of (or more easily) being characterized by Raman spectroscopy with the assistance of interference effects.[18,19] The transfer process and the chemicals used in the transfer, however, often cause damage or introduce impurities into graphene.[20] In those cases where the completeness of graphene is critical, development of techniques for characterizing as-grown graphene on Cu growth substrates is important. By imaging the birefringence of a graphene surface covered with nematic liquid crystals[21] or by annealing graphene for selective oxidation,[22] researchers have characterized graphene directly on Cu growth substrates. Though the SERS of graphene transferred onto other substrates has been studied,[23,24] the SERS of graphene as-grown on Cu foils without transfer has not been reported. Moreover, the graphene films involved in previous graphene–metal nanoparticles hybrid structures (prepared by simply covering graphene onto a metal surface or depositing metallic nano-

[a]*Department of Materials Science and Engineering & CAS Key Laboratory of Materials for Energy Conversion, University of Science and Technology of China, Hefei 230026, China. E-mail: zhuyanwu@ustc.edu.cn*
[b]*Wuxi Graphene Technologies Co., Ltd, 311 Yanxin Rd, Wuxi 214174, China*
[c]*Jiangnan Graphene Research Institute, 6 Xiangyun Rd, Changzhou 213149, China*
[d]*Collaborative Innovation Center of Chemistry for Energy Materials (2011-iChEM), Hefei 230026, China*
†Electronic supplementary information (ESI) available. See DOI: 10.1039/c4nr04225e

particles on graphene) for SERS of dye molecules are transferred from the growth substrates.[25–27] The damage and/or impurities in graphene introduced during the transfer process[20] may make it difficult to investigate the optical properties and to explore the potential applications. In addition, the SERS detection limit of 10^{-8} M for R6G molecules in our previously studied graphene–Au nanosphere hybrid system (the graphene films used were transferred from CVD grown graphene as well)[28] needs to be improved further. Therefore, studying the optical properties of graphene–metal nanostructure hybrids and pursuing their potential applications in SERS with directly grown graphene on Cu foils without transfer would be greatly desirable.

In this work, we reported largely enhanced Raman signals of graphene with the deposition of Au films on graphene grown on Cu foils with CVD. The enhancement factor (EF) was 49 fold for the 4 nm Au disposition. When the thickness of Au films was increased from 2 to 18 nm, the optical absorption of the Au/graphene/Cu hybrid platform became stronger and the plasmonic resonant wavelength showed a red shift of up to 445 nm. Finite element numerical simulations identified the role of Au Nis on graphene, leading to an efficient electric field enhancement. We have demonstrated that the hybrid structures are SERS-active substrates to detect dye molecules such as Rhodamine B (RhB), Rhodamine 6G (R6G), Sudan III and Sudan IV.

2. Experimental and methods section

Graphene was grown on Cu foils by atmospheric pressure CVD at ~1000 °C with methane as a carbon source.[10] Au films were deposited on the as-grown graphene on Cu foils at a rate of about 1 Å s^{-1} and at a pressure of about 10^{-3} Pa by plasma sputtering at room temperature. The thickness of Au films was tuned with the deposition time t (s) and current I (mA) (in the experiments, we fixed the current I to be 15 mA); thus all the thickness values reported here were calculated results of $0.007 \times It$ (nm).[29] RhB, R6G, Sudan III and Sudan IV were purchased from Sigma-Aldrich and were used without further purification. RhB, R6G, Sudan III or Sudan IV powders were dissolved in ethanol to obtain solutions with various concentrations. For SERS detection of the dye molecules, a 10 μL droplet containing different dyes was firstly hand-cast on the surface of graphene/Cu foils. Then a 4 nm Au film was deposited onto the surface of each sample after the droplet was dried in air, to protect the analyte from (or decrease) photo-induced damages such as photo-bleaching and photo-carbonization.[30] For preparing samples with two regions (half of the regions was covered with Au Nis and the rest was not covered), dust-free paper was covered on half of the regions with the analyte before depositing Au. Then the dust-free paper was peeled off before the Raman measurement. Fig. 1 schematically illustrates the fabrication procedure of the hybrid platform for optical absorption and for SERS detection.

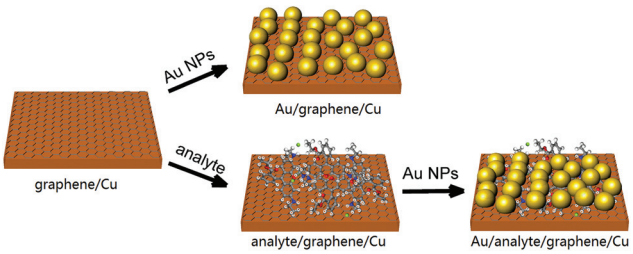

Fig. 1 Schematic illustrations of the fabrication procedure of Au/graphene/Cu structure for optical absorption and Raman detection of graphene (the top half) and Au/analyte/graphene/Cu hybrid platform for SERS of the analyte (the lower half).

Scanning electron microscopy (SEM, JSM-6700F) was used to characterize the morphology of Au films. A UV-VIS-NIR spectrometer (Solid3700, Shimadzu) was used to measure the absorbance of graphene on Cu before and after Au coating. Raman spectroscopy was performed using a Renishaw inVia Raman microscope with a 532 nm excitation laser (1 mW power) and a ×50 objective (1 μm^2 spot). The integral time was 10 s for graphene and 1 s for the samples with dye molecules. Spectral analysis was performed with a grating of 1800 lines per mm. We repeated the Raman test ten times for each position to extract the average Raman spectra.

In finite element simulations, a plane lightwave with a polarized electric field along the x-axis was launched normally from the top (as shown below in the inset of Fig. 3a). The perfectly matched layer was used for the absorbing boundary conditions in the vertical direction, while in the horizontal direction periodic boundary conditions were used to stand for an infinite Au Nis array.[31,32] The dielectric constants of Au and Cu were calculated using the Drude model,[33] and the complex refractive index $n = 3 + c_1(\lambda/3)i$ (c_1 = 5.446 μm^{-1} and λ is the wavelength) was used for graphene.[34]

3. Results and discussion

Fig. 2a shows the optical absorption spectra of Au/graphene/Cu hybrid platforms with six different thicknesses of Au films. The absorbance of bare graphene/Cu shows a strong absorption edge at wavelengths shorter than 550 nm due to the interband transitions of Cu.[35] With Au deposited on the surface of graphene/Cu, the hybrid system presents a much stronger absorption. As the Au film thickness increases, the absorption at 550 nm shows a sharp increase and then a gradual decrease (Fig. 2b). Such an observation suggests that, in addition to the absorption of Cu foils, the coupling between Au Nis and graphene may contribute to the absorption of the Au/graphene/Cu hybrid system. Thicker Au coating on the hybrid platform causes increased scattering and losses and thus reduced absorption.[24,36]

At the same time, another peak at low-energy regions is observed from the curves of Au coated hybrid structures (Fig. 2a), which corresponds to the excitation of localized surface plasmon resonance (LSPR) due to the existence of

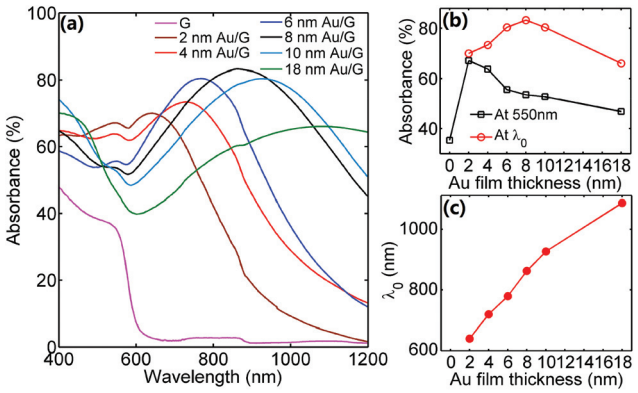

Fig. 2 (a) Absorption spectra of graphene/Cu foils before and after depositing different thicknesses of Au films. 'G' stands for graphene. (b) Absorbance values at both 550 nm and LSPR wavelength λ_0 when depositing different thicknesses of Au films. (c) Wavelength shift of LSPR with respect to the thickness of Au coating.

Au Nis.[37] The SEM images of Au coated on graphene/Cu foils shown in Fig. S1† demonstrate that the Au film essentially consists of Au Nis with the average size increasing with deposition duration of Au films. The larger nanoisland size and relatively smaller inter-island space for relatively thick Au coatings led to much stronger plasmon coupling between Au Nis.[24,30,36] However, the losses increase when the thickness of Au films is further increased in the hybrid system. The combination of increased coupling and increased loss explains the observation that the magnitude of absorbance at the resonant wavelength λ_0 first increases and then decreases with the thickness of Au films (Fig. 2b). When the Au film is thick enough, *e.g.* 18 nm in our experiments, the deposited Au tends to form a continuous film,[25] leading to the decreased absorption with weak electric field enhancement. In addition, the increased losses due to the increased scattering, grain surface effect and increase of Nis size in the thick Au films result in the decrease in the absorption and the broadening of the plasmonic peak.[36] Such an increased size of Au Nis in thicker Au films explains the red-shift in the resonant wavelength as shown in Fig. 2c.[24] The shift is up to 445 nm for the hybrid platform with Au thickness from 2 to 18 nm, making the resonant wavelength shifting from visible light to near-infrared regions, consistent with previous reports.[24,30]

Numerical simulations based on the finite element method were performed to investigate the plasmonic effects of Au Nis in the hybrid structure.[28,38–40] In a typical configuration, a periodic Au particle array with the diameter d of 24 nm and period p of 30 nm (mimicking the dimension of 4 nm Au in the experiments) was placed on the surface of the semi-infinite Cu substrate with a 1 nm thick graphene embedded in between. Fig. 3a shows the simulated absorbance as a function of incident wavelength. The normalized electrical field intensity distributions in the xz and xy planes associated with the corresponding absorption are illustrated in Fig. 3b and c. As we can see, the electric field is intensely enhanced with the existence of Au Nis. The most intense electric field is distributed at the interface between graphene and Au Nis and is confined in the vertex of Au Nis close to graphene, which is responsible for the high-energy absorption. In contrast, the low-energy resonant peak is caused by the enhanced electric field confined within the inter-space of Au Nis, which is characteristic of LSPR.[36,41] Due to the strongly enhanced electrical field at the interface of Au/graphene and between Au Nis, the absorption is largely enhanced in the hybrid system. The simulated electrical field intensity distributions for continuous Au film are shown in Fig. S2,† explaining the reduced absorption in Fig. 2b. It is worth pointing out that the calculated absorbance only gives a qualitative explanation for the experimentally observed absorption spectra; a more detailed analysis considering island distributions and different interface conditions is needed for better fitting to actual situations.

The Raman scattering of graphene has been enhanced as a result of a strongly enhanced electric field due to the presence of Au Nis, as shown in the Raman spectra in Fig. 4 for the

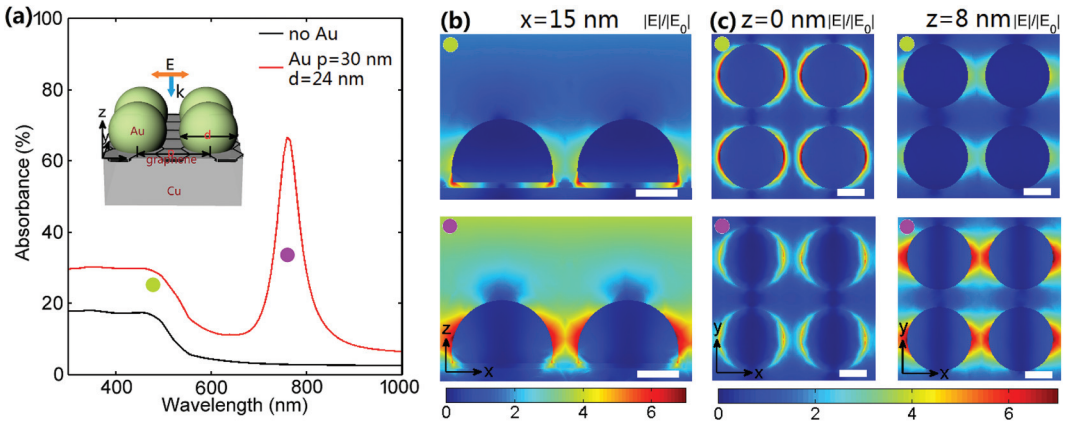

Fig. 3 (a) Calculated absorbance of graphene/Cu and Au Nis/graphene/Cu hybrid systems with Au particle period p = 30 nm, diameter d = 24 nm and a graphene thickness of 1 nm. The inset shows the configuration of Au Nis/graphene/Cu for simulations. Simulated electrical field intensity distributions in the (b) x–z plane and (c) x–y plane at z = 0 nm and z = 8 nm associated with the indicated positions in (a). In all field distribution images, the scale bar is 10 nm.

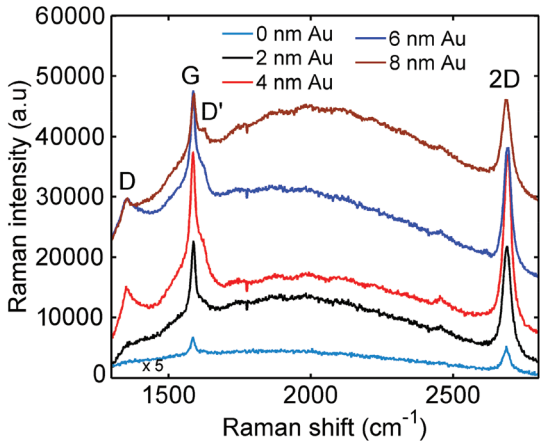

Fig. 4 Raman spectra of graphene on Cu foils before and after depositing different thicknesses of Au films.

Au/graphene/Cu hybrid platform. It was reported from the Raman spectra that the nature of graphene was not altered by depositing Au on the surface of graphene.[26] The position and full width at half maximum (FWHM) of G or 2D band are summarized in Table 1, with the EF (defined as the ratio of the intensity of G (I(G)) or 2D band (I(2D)) after Au deposition to that before Au deposition) and I(2D)/I(G) ratio presented. It can be seen that both G and 2D bands shift to larger wavenumbers after Au is coated on graphene, suggesting a p-doping in graphene.[42] This observation is consistent with previous theoretical and experimental findings that electrons are transferred from graphene to Au driven by the work function difference between Au and graphene.[43] All the 2D bands in the graphene Raman spectra exhibit a single Lorentzian shape with FWHM less than 30 cm^{-1}, which are signatures of single layer graphene.[15] The emergence of the D peak at around 1350 cm^{-1} and D′ peak at around 1620 cm^{-1} is caused by the introduction of defects during Au coating.[15,23] Similar to the absorption properties discussed in the simulation, the EF of Raman signals varies with the thickness of Au films, which can be attributed to combined effects of the coupling between graphene and Au with different Au Nis sizes and inter-island spaces, and diverse light–graphene interactions.[44] The highest EF is 49.2 for the G peak or 34.4 for the 2D peak when 4 nm Au is deposited on graphene. In this way, the Raman signals of graphene on Cu foils are largely enhanced without transfer needed, which may open up more applications of graphene on grown Cu substrates. Moreover, the EF of the G band is higher than that of the 2D band for the Au thicknesses studied, indicating that the G band is susceptible to SERS, consistent with previous reports.[23] The different response in the EF for G and 2D bands leads to the smallest value of 1.2 for the I(2D)/I(G) ratio from the hybrid platform with 4 nm Au, which might be related to the doping effect, as suggested in ref. 45.

Table 1 Position, EF, FWHM and I(2D)/I(G) ratio of graphene with different thicknesses of Au films determined from the spectra in Fig. 4

Au thickness (nm)	Position (cm^{-1})		EF		FWHM (cm^{-1})		
	G band	2D band	G band	2D band	G band	2D band	I(2D)/I(G)
0	1585	2687	—	—	20	29	1.7
2	1587	2690	25.2	23.4	22	28	1.6
4	1587	2691	49.2	34.5	28	26	1.2
6	1588	2694	35.2	26.4	26	27	1.3
8	1590	2692	19.7	18.7	20	30	1.6

The enhanced absorption and Raman scattering of the hybrid platform make them suitable substrates for SERS. Fig. 5a shows the SERS spectra of RhB imbedded between Au and graphene/Cu with concentrations increasing from 1×10^{-10} to 1×10^{-5} M. The Raman signal is still observable for molecule concentrations down to 10^{-10} M. Fig. 5b plots the SERS intensity at 1649 cm^{-1} depending on the concentration of RhB and a more detailed curve for Raman intensity and molecular concentration is shown in Fig. S3.† The detection limit of 10^{-10} M was also obtained from R6G on the hybrid substrate (Fig. S4, ESI†). The detection limit of 10^{-10} M for R6G in the proposed structure has a ~100-fold decrease compared to our previously studied graphene–Au nanosphere hybrid system (the detection limit for R6G is 10^{-8} M),[28] indicating highly improved sensitivity. The higher sensitivity is considered to be caused by the coupling effect between Au Nis and graphene on Cu foils with a strong electric field enhancement.[46,47] By embedding an analyte between graphene and Au, the hybrid system could protect the analyte from (or decrease) photo-induced damage and make the analyte have better contact with graphene to further improve the sensitivity as the chemical enhancement arising from π–π staking and charge transfer between graphene and dye molecules may benefit the Raman enhancement.[28,47] The Raman spectra of 10^{-2} M RhB and R6G on graphene/Cu foils without Au deposition are compared in Fig. S5.† The SERS EF has been defined by EF = $(I_{SERS}/I_{bulk}) \times (N_{bulk}/N_{SERS})$,[48] where I_{SERS} and I_{bulk} are the peak intensities of the 10^{-9} M in 4 nm Au/analyte/graphene/Cu foils and 10^{-2} M on graphene/Cu foils at 1649 cm^{-1} for RhB or 612 cm^{-1} for R6G, N_{SERS} and N_{bulk} are the numbers of RhB or R6G molecules excited by the laser beam in the hybrid platform and on the graphene/Cu foils, respectively. In this way, the calculated EFs are 5.14×10^6 for RhB and 8.46×10^6 for R6G, respectively. The 4 nm Au/graphene/Cu foil was also employed to detect Sudan dyes. Sudan dyes are classified as category 3 carcinogens by the International Agency for Research on Cancer (IARC) due to the fact that they are suspected of being human carcinogens though they are widely used as food additives.[49] The Raman spectra in Fig. 5c and d show that both Sudan III and Sudan IV can be detected on the hybrid platform with a concentration of as low as 10^{-10} M as well. The intensity *versus* concentration curves for both Sudan III and Sudan IV are shown in Fig. S6,† presenting a similar trend with RhB. Considering the largely lowered CVD production cost of graphene on Cu and the no-transfer technique we proposed, the detection limit of 0.1 nM for RhB, R6G, Sudan III and Sudan IV could be valuable when compared to those reported with a similar metal morphology for dye molecule detection.[28,50,51]

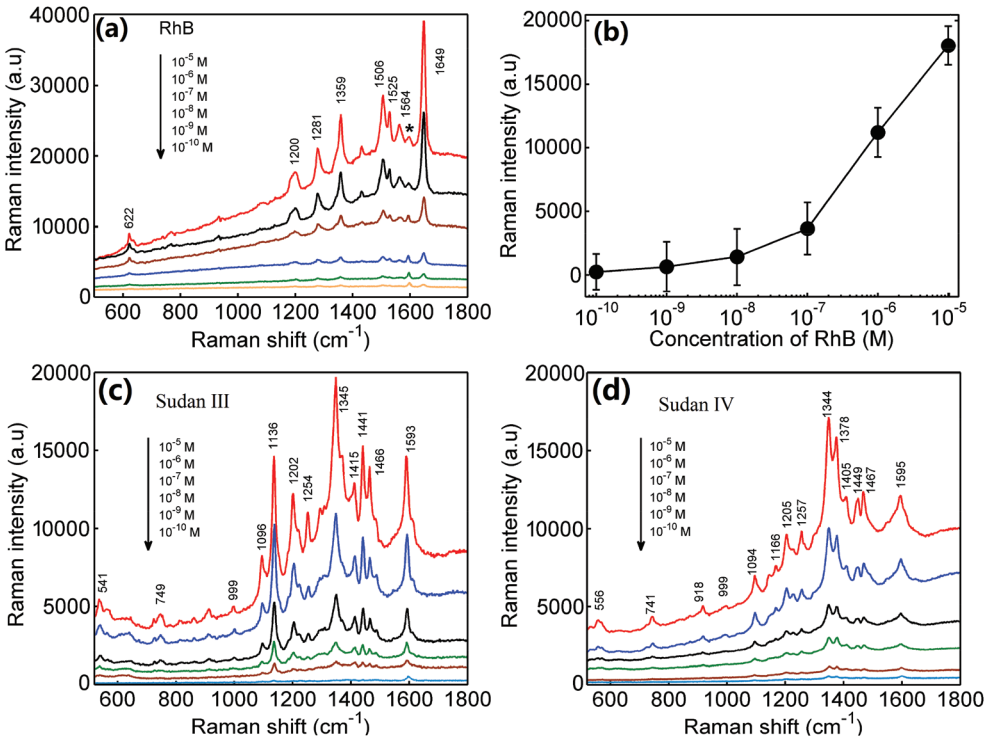

Fig. 5 (a) SERS spectra of RhB (4 nm Au/RhB/graphene/Cu) with six different molecular concentrations. * marks the G band of graphene. (b) The intensity of SERS signal at 1649 cm^{-1} *versus* the concentration of RhB. SERS spectra of (c) Sudan III (4 nm Au/Sudan III/graphene/Cu) and (d) Sudan IV (4 nm Au/Sudan IV/graphene/Cu) with six different molecular concentrations.

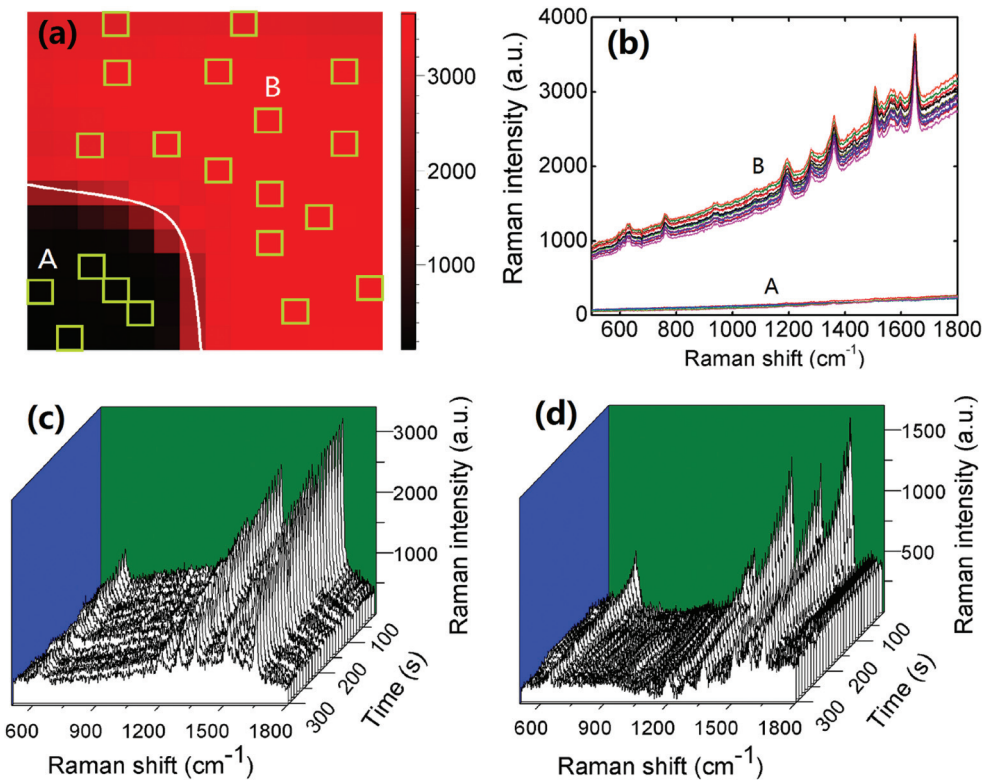

Fig. 6 (a) Spatial resolved Raman intensity mappings of the 1649 cm^{-1} peak of 10^{-7} M RhB on the Au-graphene/Cu hybrid system with (region B) and without 4 nm Au (region A) on the surface. (b) Raman spectra of 10^{-7} M RhB taken from the mapping area of (a) marked by boxes containing both regions A and B. Stability of (c) 10^{-7} M RhB in the structure of 4 nm Au/RhB/graphene/Cu and (d) 10^{-2} M RhB on the surface of graphene/Cu foils, respectively.

Uniformity, reliability and stability are critical for the practical application of SERS substrates. Fig. 6a shows the Raman intensity mapping image of 10^{-7} M RhB at 1649 cm^{-1} in the area of 14 × 14 μm^2 on the RhB/graphene/Cu foils (region A) and on 4 nm Au/RhB/graphene/Cu foils (region B). With such a low concentration, the Raman signals of RhB are not distinguished on the RhB/graphene/Cu foils while they show highly consistent curves from different sites (Fig. 6b) on Au/RhB/graphene/Cu foils. The higher sensitivity for region B than region A clearly demonstrates that the strongly enhanced electric field due to the presence of Au Nis plays an important role for improved SERS intensity, which is consistent with previous reports.[30,47] The time-dependent measurement was carried out on the SERS of 10^{-7} M RhB on 4 nm Au/graphene/Cu foils or on that of 10^{-2} M RhB on graphene/Cu foils for 300 s, as shown in Fig. 6c and d. It can be seen that the Raman intensity decreases quickly on graphene/Cu foils, but it is more stable on 4 nm Au/graphene/Cu foils.

4. Conclusions

In conclusion, we have developed a simple method to enhance the Raman signals of as-grown graphene on Cu foils. An enhancement in graphene Raman signal of up to 49 fold has been achieved by depositing a 4 nm thick Au film due to the coupling between graphene and the plasmonic modes of Au Nis. The plasmonic effect of the Au/graphene/Cu hybrid platform has led to the strong absorption at the resonant wavelength and the significant red shift in resonant wavelength when the thickness of Au films is increased from 2 to 18 nm. Finite element numerical simulations identified the role of Au Nis on graphene, leading to an efficient electric field enhancement. In addition, the hybrid systems have been used as SERS-active substrates, which shows an enhancement of $\sim 10^6$ for RhB and R6G with uniform and stable response and a detection limit of as low as 0.1 nM for Sudan III and Sudan IV. The results may demonstrate promising applications for SERS detection and open up new opportunities in developing more applications of as-grown graphene on Cu foils.

Acknowledgements

Y. Zhu appreciates the financial support from the China Government 1000 Plan Talent Program, China MOE NCET Program, Natural Science Foundation of China (51322204) and the Fundamental Research Funds for the Central Universities (WK2060140014).

Notes and references

1 H. Yan, X. Li, B. Chandra, G. Tulevski, Y. Wu, M. Freitag, W. Zhu, P. Avouris and F. Xia, *Nat. Nanotechnol.*, 2012, **7**, 330–334.
2 Z. Fei, A. S. Rodin, G. O. Andreev, W. Bao, A. S. McLeod, M. Wagner, L. M. Zhang, Z. Zhao, M. Thiemens, G. Dominguez, M. M. Fogler, A. H. C. Neto, C. N. Lau, F. Keilmann and D. N. Basov, *Nature*, 2012, **487**, 82–85.
3 P. Alonso-Gonzalez, A. Y. Nikitin, F. Golmar, A. Centeno, A. Pesquera, S. Velez, J. Chen, G. Navickaite, F. Koppens, A. Zurutuza, F. Casanova, L. E. Hueso and R. Hillenbrand, *Science*, 2014, **344**, 1369–1373.
4 F. H. L. Koppens, D. E. Chang, S. Thongrattanasiri and F. J. G. Garcia de Abajo, *Opt. Photonics News*, 2011, **22**, 36.
5 L. Shao, X. Wang, H. Xu, J. Wang, J.-B. Xu, L.-M. Peng and H.-Q. Lin, *Adv. Opt. Mater*, 2014, **2**, 162–170.
6 R. Jiang, B. Li, C. Fang and J. Wang, *Adv. Mater.*, 2014, **26**, 5274–5309.
7 K. V. Emtsev, A. Bostwick, K. Horn, J. Jobst, G. L. Kellogg, L. Ley, J. L. McChesney, T. Ohta, S. A. Reshanov, J. Roehrl, E. Rotenberg, A. K. Schmid, D. Waldmann, H. B. Weber and T. Seyller, *Nat. Mater.*, 2009, **8**, 203–207.
8 Y. Zhu, S. Murali, W. Cai, X. Li, J. W. Suk, J. R. Potts and R. S. Ruoff, *Adv. Mater.*, 2010, **22**, 3906–3924.
9 A. Reina, X. Jia, J. Ho, D. Nezich, H. Son, V. Bulovic, M. S. Dresselhaus and J. Kong, *Nano Lett.*, 2009, **9**, 30–35.
10 X. Li, W. Cai, J. An, S. Kim, J. Nah, D. Yang, R. Piner, A. Velamakanni, I. Jung, E. Tutuc, S. K. Banerjee, L. Colombo and R. S. Ruoff, *Science*, 2009, **324**, 1312–1314.
11 Y. Hao, M. S. Bharathi, L. Wang, Y. Liu, H. Chen, S. Nie, X. Wang, H. Chou, C. Tan, B. Fallahazad, H. Ramanarayan, C. W. Magnuson, E. Tutuc, B. I. Yakobson, K. F. McCarty, Y.-W. Zhang, P. Kim, J. Hone, L. Colombo and R. S. Ruoff, *Science*, 2013, **342**, 720–723.
12 S. Bae, H. Kim, Y. Lee, X. Xu, J.-S. Park, Y. Zheng, J. Balakrishnan, T. Lei, H. R. Kim, Y. I. Song, Y.-J. Kim, K. S. Kim, B. Ozyilmaz, J.-H. Ahn, B. H. Hong and S. Iijima, *Nat. Nanotechnol.*, 2010, **5**, 574–578.
13 O. Frank, J. Vejpravova, V. Holy, L. Kavan and M. Kalbac, *Carbon*, 2014, **68**, 440–451.
14 A. C. Ferrari, J. C. Meyer, V. Scardaci, C. Casiraghi, M. Lazzeri, F. Mauri, S. Piscanec, D. Jiang, K. S. Novoselov, S. Roth and A. K. Geim, *Phys. Rev. Lett.*, 2006, **97**, 187401.
15 A. C. Ferrari and D. M. Basko, *Nat. Nanotechnol.*, 2013, **8**, 235–246.
16 S. D. Costa, A. Righi, C. Fantini, Y. Hao, C. Magnuson, L. Colombo, R. S. Ruoff and M. A. Pimenta, *Solid State Commun.*, 2012, **152**, 1317–1320.
17 G. V. Troppenz, M. A. Gluba, M. Kraft, J. Rappich and N. H. Nickel, *J. Appl. Phys.*, 2013, **114**, 214312.
18 P. Blake, E. W. Hill, A. H. C. Neto, K. S. Novoselov, D. Jiang, R. Yang, T. J. Booth and A. K. Geim, *Appl. Phys. Lett.*, 2007, **91**, 214312.
19 P. Klar, E. Lidorikis, A. Eckmann, I. A. Verzhbitskiy, A. C. Ferrari and C. Casiraghi, *Phys. Rev. B: Condens. Matter*, 2013, **87**, 205435.
20 A. Pirkle, J. Chan, A. Venugopal, D. Hinojos, C. W. Magnuson, S. McDonnell, L. Colombo, E. M. Vogel, R. S. Ruoff and R. M. Wallace, *Appl. Phys. Lett.*, 2011, **99**, 122108.

21 K. Dae Woo, K. Yun Ho, J. Hyeon Su and J. Hee-Tae, *Nat. Nanotechnol.*, 2012, **7**, 29–34.
22 C. Jia, J. Jiang, L. Gan and X. Guo, *Sci. Rep.*, 2012, **2**, 707.
23 J. Lee, S. Shim, B. Kim and H. S. Shin, *Chem. – Eur. J.*, 2011, **17**, 2381–2387.
24 G. Xu, J. Liu, Q. Wang, R. Hui, Z. Chen, V. A. Maroni and J. Wu, *Adv. Opt. Mater.*, 2012, **24**, OP71–OP76.
25 Y. Wang, Z. Ni, H. Hu, Y. Hao, C. P. Wong, T. Yu, J. T. L. Thong and Z. X. Shen, *Appl. Phys. Lett.*, 2010, **97**, 163111.
26 H. Zhou, C. Qiu, Z. Liu, H. Yang, L. Hu, J. Liu, H. Yang, C. Gu and L. Sun, *J. Am. Chem. Soc.*, 2010, **132**, 944–946.
27 N. Reckinger, A. Vlad, S. Melinte, J.-F. Colomer and M. Sarrazin, *Appl. Phys. Lett.*, 2013, **102**, 211108.
28 Y. Du, Y. Zhao, Y. Qu, C.-H. Chen, C.-M. Chen, C.-H. Chuang and Y. Zhu, *J. Mater. Chem. C*, 2014, **2**, 4683–4691.
29 Plasma Sputter Coating. http://www.mtixtl.com/desk-top-plasmasputteringcoaterformetallic-coatingwithvacuum-pumpandgoldtarget15maxsample.aspx, MTI Corporation.
30 W. Xu, X. Ling, J. Xiao, M. S. Dresselhaus, J. Kong, H. Xu, Z. Liu and J. Zhang, *Proc. Natl. Acad. Sci. U. S. A.*, 2012, **109**, 9281–9286.
31 J. C. Chen and K. Li, *Microw. Opt. Technol. Lett.*, 1995, **10**, 319–323.
32 Y. Zhao, G. Chen, Z. Tao, C. Zhang and Y. Zhu, *RSC Adv.*, 2014, **4**, 26535–26542.
33 E. J. Zeman and G. C. Schatz, *J. Phys. Chem.*, 1987, **91**, 634–643.
34 M. Bruna and S. Borini, *Appl. Phys. Lett.*, 2009, **94**, 031901.
35 K. Schroder and D. Onengut, *Phys. Rev.*, 1967, **162**, 628–631.
36 H.-Y. Wu, C. J. Choi and B. T. Cunningham, *Small*, 2012, **8**, 2878–2885.
37 L. Seungwoo, L. Min hyung, S. Hyeon-jin and C. Dukyun, *Nanotechnology*, 2013, **24**, 275702.
38 A. V. Krasavin and A. V. Zayats, *Phys. Rev. B: Condens. Matter*, 2008, **78**, 045425.
39 Y. Zhao, X. Hu, G. Chen, X. Zhang, Z. Tan, J. Chen, R. S. Ruoff, Y. Zhu and Y. Lu, *Phys. Chem. Chem. Phys.*, 2013, **15**, 17118–17125.
40 *COMSOL 4.3a Reference Manual*, 2012, 4.3.
41 E. Hutter and J. H. Fendler, *Adv. Mater.*, 2004, **16**, 1685–1706.
42 J. Lee, K. S. Novoselov and H. S. Shin, *ACS Nano*, 2011, **5**, 608–612.
43 G. Giovannetti, P. A. Khomyakov, G. Brocks, V. M. Karpan, J. van den Brink and P. J. Kelly, *Phys. Rev. Lett.*, 2008, **101**, 026803.
44 X. Zhu, L. Shi, M. S. Schmidt, A. Boisen, O. Hansen, J. Zi, S. Xiao and N. A. Mortensen, *Nano Lett.*, 2013, **13**, 4690–4696.
45 A. Das, S. Pisana, B. Chakraborty, S. Piscanec, S. K. Saha, U. V. Waghmare, K. S. Novoselov, H. R. Krishnamurthy, A. K. Geim, A. C. Ferrari and A. K. Sood, *Nat. Nanotechnol.*, 2008, **3**, 210–215.
46 J. Mertens, A. L. Eiden, D. O. Sigle, F. Huang, A. Lombardo, Z. Sun, R. S. Sundaram, A. Colli, C. Tserkezis, J. Aizpurua, S. Milana, A. C. Ferrari and J. J. Baumberg, *Nano Lett.*, 2013, **13**, 5033–5038.
47 X. Li, W. C. H. Choy, X. Ren, D. Zhang and H. Lu, *Adv. Funct. Mater.*, 2014, **24**, 3114–3122.
48 L. Zhang, C. Jiang and Z. Zhang, *Nanoscale*, 2013, **5**, 3773–3779.
49 N. A. G. A. Refat, Z. S. Ibrahim, G. G. Moustafa, K. Q. Sakamoto, M. Ishizuka and S. Fujita, *J. Biochem. Mol. Toxicol.*, 2008, **22**, 77–84.
50 X. Zhou, F. Yan and P. Zhang, *Trends Appl. Sci. Res.*, 2006, **1**, 155–161.
51 C. Qiu, H. Zhou, B. Cao, L. Sun and T. Yu, *Carbon*, 2013, **59**, 487–494.

